# NON-NEWTONIAN FLUID FLOW IN AN ECCENTRIC ANNULUS*

NOBUO MITSUISHI AND YOSHIKI AOYAGI**
*Department of Nuclear Engineering, Kyushu University, Fukuoka, Japan*

**Non-Newtonian fluid flow in an eccentric annulus was studied for high polymer aqueous solutions of CMC, HEC and MC. The macroscopic relations between the pressure drop and the flow rate were found to be in fairly good agreement with the results obtained by application of the conventional variational principle.**

**Velocity profiles were measured by a hydrogen bubble method in which photographs were taken of the hydrogen bubbles. The authors observed very interesting secondary flows in the eccentric non-Newtonian fluid flow which may be due to the viscoelastic effect of the high polymer aqueous solution. The authors could not observe such secondary flows for non-Newtonian fluids in a concentric annulus or Newtonian fluids in an eccentric annulus.**

**The authors present an equation giving the relation between the flow rate and the pressure drop for the flow of a non-Newtonian fluid in an eccentric annulus in terms of the experimental data for flow in a circular tube.**

## Introduction

A large number of studies have investigated fluid flow and heat transfer in a concentric annulus, while only a limited number of studies have been carried out on non-Newtonian fluid flow and heat transfer in an eccentric annulus. The latter may be important for the case of fluid flow in the die of an extruder.

N.A.Y. Piercy *et al.*[9] and others[10,13,15] have investigated Newtonian flow in an eccentric annulus, but very little work has been done on non-Newtonian flow in such a geometry. This paper presents both the theoretical and experimental results of flow rate, pressure drop, and velocity profiles for non-Newtonian flow in an eccentric annulus under steady-state conditions. Since the basic equations for non-Newtonian fluid flow in an eccentric annulus are non-linear partial differential equations, it is very difficult to obtain an analytical solution by classical methods. Therefore, with a few exceptions[3], one usually uses an approximate method such as the variational method for non-Newtonian flow problems. For example, Shechter[11] presented non-Newtonian flow in a rectangular duct, and the authors[4,7,8] presented non-Newtonian flow in elliptical, triangular, and rectangular ducts.

This paper presents a comparison of the experimental data with the conventional variational method analysis for fluid flow in an eccentric annulus, using the 3-constant Sutterby model[14] as a non-Newtonian model. The velocity profiles were measured by a hydrogen bubble method in which photographs were taken of the hydrogen bubbles. The authors observed a secondary flow in the eccentric annulus for a non-Newtonian flow which may be due to the viscoelastic effect of the non-Newtonian fluid. Furthermore, an equation is given to predict the relation between flow rate and pressure drop in an eccentric annulus in terms of the experimental fluid flow data in a circular tube.

## 1. Theoretical Consideration

For mathematical simplicity, it is better to use bi-

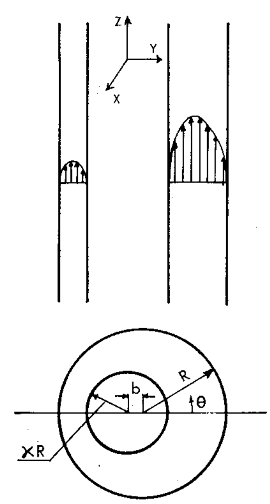


**Fig. 1 Flow in an eccentric annulus**

* Received on February 19, 1973
Presented at American Rheology Meeting in Cincinnati, Ohio, U.S.A. (January 31, 1973)
** Mitsubishi Chemical Co., Ltd.
〒812 福岡市東区箱崎町
九州大学工学部応用原子核工学教室 三石信雄

polar coordinates[2)] as shown in **Fig. 2** for the analysis of fluid flow in an eccentric annulus. For bipolar cylindrical coordinates, the variables $(\xi, \zeta, z)$ are related to rectangular coordinates $(x, y, z)$ as follows:

$$x+iy=iC\cot((\xi+i\zeta)/2) \tag{1}$$

$$z=z \tag{2}$$

where $i$ is $\sqrt{-1}$.
Elimination of $\xi$ in Eq.(1) results in

$$(x-C\coth\zeta)^2+y^2=C^2/\sinh^2\zeta \tag{3}$$

For constant $\zeta$, this equation describes a circle, where the coordinates of the center are $(C\coth\zeta, 0)$ and the radius is $C/\sinh\zeta$. Therefore, the inner and outer walls of the eccentric annulus can be expressed by constant values of $\zeta_i$ and $\zeta_0$, respectively, since these are circles.
As in Fig. 2

$$\kappa R=C/\sinh\zeta_i \tag{4}$$

$$R=C/\sinh\zeta_0 \tag{5}$$

$$b=C(\coth\zeta_0-\coth\zeta_i) \tag{6}$$

Where $\kappa$ is the ratio of inner to outer radius. The eccentric ratio is defined as follows:

$$e=b/R(1-\kappa) \tag{7}$$

The relations between $(C, \zeta_i, \zeta_0)$ and $(R, \kappa, e)$ are

$$\cosh\zeta_i=[1+\kappa-(1-\kappa)e^2]/2\kappa e \tag{8}$$

$$\cosh\zeta_0=[1+\kappa+(1-\kappa)e^2]/2e \tag{9}$$

$$C=R\sinh\zeta_0 \tag{10}$$

Therefore, the size of a double tube, $(R, \kappa, e)$ determines the coordinates mentioned above. The scale factors in the bipolar cylindrical coordinate system are

$$h_\xi=h_\zeta=(\cosh\zeta-\cos\xi)/C\equiv h \tag{11}$$

$$h_z=1 \tag{12}$$

The equation of motion for steady laminar flow is

$$-\tau_{ij,j}-p_i+\rho g_i=\rho v_{i,j}v_j \tag{13}$$

The equation of continuity, assuming incompressible fluid flow, is

$$v_{i,i}=0 \tag{14}$$

The rheological equation between components of the stress tensor and the rate of deformation tensor is

$$\tau_{ij}=-2\eta d_{ij} \tag{15}$$

For the Sutterby model

$$\eta=\eta_0[(\mathrm{arcsinh}B\sqrt{2\mathrm{II}})/B\sqrt{2\mathrm{II}}]^A \tag{16}$$

where

$$\mathrm{II}=d_{ij}d_{ji} \tag{17}$$

$$d_{ij}=(v_{i,j}+v_{j,i})/2 \tag{18}$$

These equations are rewritten in the bipolar cylindrical coordinate system in order to simplify the analysis for flow in an eccentric annulus. The velocity components in this case are

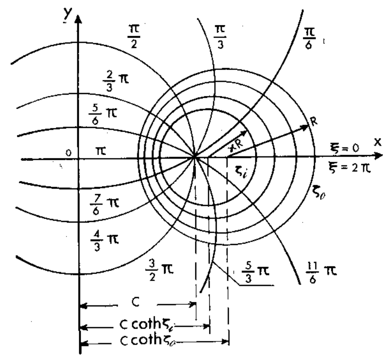


**Fig. 2 Bipolar cylindrical coordinate**

$$v_\xi=v_\zeta=0 \tag{19}$$

$$v_z=v(\xi, \zeta) \tag{20}$$

The non-zero components for the rate of deformation tensor are

$$d_{\xi z}=d_{z\xi}=\frac{1}{2}h\frac{\partial v}{\partial \xi} \tag{21}$$

$$d_{\zeta z}=d_{z\zeta}=\frac{1}{2}h\frac{\partial v}{\partial \zeta} \tag{22}$$

The second invariant of $d_{ij}$, II is

$$\mathrm{II}=\frac{h^2}{2}\left\{\left(\frac{\partial v}{\partial \xi}\right)^2+\left(\frac{\partial v}{\partial \zeta}\right)^2\right\} \tag{23}$$

The equations of motion are

$$\xi\text{—component:}\quad \partial\tau_{\xi z}/\partial z+h\partial p/\partial\xi=0 \tag{24}$$

$$\zeta\text{—component:}\quad \partial\tau_{\zeta z}/\partial z+h\partial p/\partial\zeta=0 \tag{25}$$

$z$—component:

$$h^2\left\{\frac{\partial}{\partial\xi}\left(\frac{\partial\tau_{\xi z}}{h}\right)+\frac{\partial}{\partial\zeta}\left(\frac{\tau_{\zeta z}}{h}\right)\right\}+\frac{\partial p}{\partial z}-\rho g_z=0 \tag{26}$$

Since $\tau_{\xi z}$ and $\tau_{\zeta z}$ are not functions of $z$, from Eqs.(24) and (25).

$$\frac{\partial p}{\partial \xi}=\frac{\partial p}{\partial \zeta}=0 \tag{27}$$

Hence $p$ is only a function of $z$. The first term in Eq.(26) is a function of $\xi$ and $\zeta$, and the rest of the terms depend on $z$. The equation may be expressed as

$$h^2\left\{\frac{\partial}{\partial\xi}\left(\frac{\tau_{\xi z}}{h}\right)+\frac{\partial}{\partial\zeta}\left(\frac{\partial\tau_{\xi z}}{h}\right)\right\}=-\frac{\partial p}{\partial z}+\rho g_z\equiv\frac{\Delta P}{L} \tag{28}$$

Eqs.(15), (16), (21), (22), (23) and (28) are to be solved with the boundary conditions

$$\text{at}\quad \zeta=\zeta_i \quad\text{and}\quad \zeta=\zeta_0,\quad v=0 \tag{29}$$

$$\text{at}\quad \xi=0 \quad\text{and}\quad \xi=\pi,\quad \partial v/\partial\xi=0 \tag{30}$$

It is very difficult to get an analytical solution for these non-linear partial differential equations. Instead, we will get an approximate solution by using the variational method.

## 2. Analysis by the Variational Method

We consider the variational problem which has the functional

$$J=\int_0^{\pi}\int_{\zeta_0}^{\zeta_i}\left\{\int_0^{\mathrm{II}}\eta d\mathrm{II}-\frac{\Delta P}{L}v\right\}\frac{d\zeta d\xi}{h^2} \tag{31}$$

where the velocity profile $v$ must satisfy the boundary conditions of Eqs.(29) and (30). Using Eqs.(15), (21) and (22), we get the variational $\delta J$ of Eq.(31) as follows:

$$\delta J=\int_0^{\pi}\int_{\zeta_0}^{\zeta_i}\left\{h^2\left[\frac{\partial}{\partial\xi}\left(\frac{\tau_{\xi z}}{h}\right)+\frac{\partial}{\partial\zeta}\left(\frac{\tau_{\zeta z}}{h}\right)\right]-\frac{\Delta P}{L}\right\}\delta v\frac{\partial\zeta\partial\xi}{h^2} \tag{32}$$

If the functional $J$ takes an extreme value, that is, if $\delta J=0$, the following equation is obtained.

$$h^2\left[\frac{\partial}{\partial\xi}\left(\frac{\tau_{\xi z}}{h}\right)+\frac{\partial}{\partial\zeta}\left(\frac{\tau_{\zeta z}}{h}\right)\right]-\frac{\Delta P}{L}=0 \tag{33}$$

This equation corresponds to Eq.(28). Hence Eq.(31) is the functional equivalent to the foregoing boundary value problem. We follow Ritz's method[12] to obtain the velocity distribution which minimizes the $J$ of Eq.(31), and satisfies the boundary conditions of Eqs.(29) and (30). We presented in a previous paper[6] a macroscopic relation between flow rate and pressure drop accurate to the first approximation which may be sufficient for practical usage. We assume here a trial function for the velocity distribution which has three undetermined multipliers.

$$\begin{aligned}v^*&=v/[C^2\Delta P/\eta_0 L]\\&=a_1v_1^*+a_2v_2^*+a_3v_3^*\end{aligned} \tag{34}$$

where

$$\begin{aligned}v_1^*=&\{(\zeta-\zeta_0)\coth\zeta_i+(\zeta_i-\zeta)\coth\zeta_0\}/2(\zeta_i-\zeta_0)\\&-\cosh\zeta/2(\cosh\zeta-\cos\xi)\\&+\sum_{1,3,\dots}^{\infty}[\cos n\xi\{e^{-n\zeta_i}\coth\zeta_i\sinh n(\zeta-\zeta_0)\\&+e^{-n\zeta_0}\coth\zeta_0\sinh n(\zeta_i-\zeta)\}/\sinh n(\zeta_i-\zeta_0)]\end{aligned} \tag{35}$$

$$v_2^*=(\zeta-\zeta_i)^2(\zeta-\zeta_0)^2 \tag{36}$$

$$v_3^*=(\zeta-\zeta_i)^2(\zeta-\zeta_0)^2\cos\xi \tag{37}$$

Substitution of Eqs.(16), (23), (34) into Eq.(31), and making use of

$$\partial J/\partial a_i=0 \qquad (i=1, 2, 3) \tag{38}$$

which is a condition of taking an extreme value, results in

$$\int_0^{\pi}\int_{\zeta_0}^{\zeta_i}\frac{1}{h^{*2}}\left(\frac{\partial\mathrm{II}^*}{\partial a_i}\eta^*-v_1^*\right)d\zeta d\xi=0 \qquad (i=1, 2, 3) \tag{39}$$

where

$$h^*=Ch=\cosh\zeta-\cos\xi \tag{40}$$

$$\mathrm{II}^*=h^{*2}\left[\left(\frac{\partial v^*}{\partial\xi}\right)^2+\left(\frac{\partial v^*}{\partial\zeta}\right)^2\right] \tag{41}$$

$$\eta^*=[\mathrm{arcsinh}\,\tau^*\sqrt{\mathrm{II}^*}/\tau^*\sqrt{\mathrm{II}^*}]^A \tag{42}$$

$$\tau^*=\frac{B}{\eta_0}\frac{C\Delta P}{L} \tag{43}$$

The solution to the simultaneous set of equations, Eq.(39), gives the $a_i$'s as a function of $\tau^*$ and the model parameter A. The definite integral appearing in Eq.(39) was numerically calculated using a digital computer. Substitution of the $a_i$'s, obtained as mentioned above, into Eq.(34) gives the velocity distribution. The flow rate is obtained by summing up the velocity distribution over a cross section of the duct.

Finally, the reduced flow rate $Q^*$ and the reduced pressure drop $P^*$ are as follows:

$$Q^*\equiv B(4Q/\pi R^3)=8\tau^*\nu^3\int_0^{\pi}\int_{\zeta_0}^{\zeta_i}v^*/h^{*2}d\zeta d\xi \tag{44}$$

$$P^*\equiv(B/\eta_0)(R\Delta P/2L)=\tau^*/2\nu \tag{45}$$

where

$$\nu=C/R=\sinh\zeta_0 \tag{46}$$

From the above equations, the relation between pressure drop and velocity distribution, and that between pressure drop and flow rate can be obtained. **Figure 3** shows an example of the velocity distribution, and **Fig. 4** shows an example of the relation between flow rate and pressure drop. The contribution of eccentric ratio to pressure drop is shown in **Fig. 5**.

## 3. Prediction of the Flow in an Eccentric Annulus in Terms of Circular Tube Data

By the same procedure as presented in our previous paper,[7] we set up a useful empirical equation which can estimate the relation between flow rate and pressure drop for the eccentric flow in terms of the data for the flow in a circular tube.

The reduced flow rate $Q_c^*$ and the reduced pressure drop $P_c^*$ in a circular tube may be approximately related to those of $Q^*$ and $P^*$ in an eccentric annulus by the following equations.

$$Q^*=G(\kappa, e)Q_c^* \tag{47}$$

$$P^*=F(\kappa, e)P_c^* \tag{48}$$

$G(\kappa, e)$ and $F(\kappa, e)$, obtained as in the previous paper, are given in **Table 1**. $G$ and $F$ may be expressed within several percent error by the following equations, which are functions of $\kappa$ and $e$.

$$\begin{aligned}F=&\{1.020+0.0946\kappa-0.135\kappa^2+(-0.143-0.284\kappa\\&+0.213\kappa^2)e+(0.0871-0.758\kappa\\&+0.480\kappa^2)e^2\}/(1-\kappa)\end{aligned} \tag{49}$$

$$\begin{aligned}G=&\{0.734-0.125\kappa-0.615\kappa^2-(0.0403+0.0984\kappa\\&+0.0567\kappa^2)e+(0.470-0.231\kappa\\&-0.247\kappa^2)e^2\}(1-\kappa)\end{aligned} \tag{50}$$

**Table 1 Numerical values of $F(\kappa, e)$ and $G(\kappa, e)$**

| $\kappa$ | $e$ | 0.0 | 0.2 | 0.4 | 0.6 | 0.8 |
|---|---|---|---|---|---|---|
| 0.2 | $F$ | 1.28 | 1.26 | 1.19 | 1.11 | 1.08 |
| | $G$ | 0.545 | 0.561 | 0.594 | 0.650 | 0.747 |
| 0.4 | $F$ | 1.72 | 1.68 | 1.54 | 1.40 | 1.29 |
| | $G$ | 0.351 | 0.361 | 0.382 | 0.419 | 0.478 |
| 0.6 | $F$ | 2.54 | 2.48 | 2.25 | 2.01 | 1.82 |
| | $G$ | 0.174 | 0.180 | 0.190 | 0.208 | 0.237 |
| 0.8 | $F$ | 5.01 | 4.88 | 4.39 | 3.90 | 3.47 |
| | $G$ | 0.0481 | 0.0496 | 0.0523 | 0.0575 | 0.0649 |

**Table 2 Sizes of eccentric annuli used in experiments**

| No. | $R$ [cm] | $b$ [cm] | $\kappa$ [—] | $e$ [—] |
|---|---|---|---|---|
| 1 | 0.921 | 0.145 | 0.635 | 0.430 |
| 2 | 0.757 | 0.194 | 0.526 | 0.541 |
| 3 | 0.757 | 0.331 | 0.328 | 0.650 |
| 4 | 0.757 | 0.203 | 0.526 | 0.565 |
| 5 | 0.921 | 0.523 | 0.432 | 1.000 |
| 6 | 1.387 | 0.466 | 0.359 | 0.524 |

where

$$0.2 \leq \kappa \leq 0.8 \quad \text{and} \quad 0.0 \leq e \leq 0.8$$

In the case of $e=0$, these equations reduce to those for a concentric annulus given in our previous paper. **Figure 6** shows a comparison between the $P^*$ vs. $Q^*$ flow curve (solid line) and the $FP_c^*$ vs. $GQ_c^*$ flow curve (dotted line) which were obtained by the method mentioned in the previous section and by Eqs.(47) and (48), respectively, where $\kappa=0.4$ and $e=0.6$. For values of $A$ less than 0.6, these curves agree quite well. Under ordinary circumstances, these equations may be useful in estimating the relation between pressure drop and flow rate, since high polymer solutions have the value of $A$ in the range of 0.0~0.7. By these equations, the relation between flow rate and pressure drop in an eccentric annulus may be estimated in terms of the experimental data for flow in a circular tube.

## 4. Comparison of the Experimental Data with the Calculated Results

The experimental apparatus and the method of measurement are almost the same as in the previous paper[7]. **Table 2** shows the dimensions of the eccentric tubes used. These dimensions were determined experimentally by using a Newtonian fluid of known viscosity, and agree approximately with those measured by gauge. In order to accurately observe the velocity profiles, the larger tubes, No. 6 in Table 2, were used. Hydrogen bubbles were generated as tracers and photographs were taken using a camera and stroboscope arrangement. The velocity profiles were observed at the points where the clearance between the inner and outer tubes are a maximum ($\theta=0°$), a minimum ($\theta=180°$), and two values intermediate between the two ($\theta=60°$, $\theta=120°$) (see Fig. 9). A square pillar filled with water was installed outside of the No. 6 double tubes so as to minimize the effect of refraction.

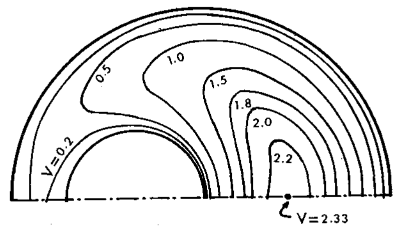

**Fig. 3 Flow curves for Sutterby model fluids flowing in an eccentric annulus ($\kappa=0.6$, $e=0.4$)**

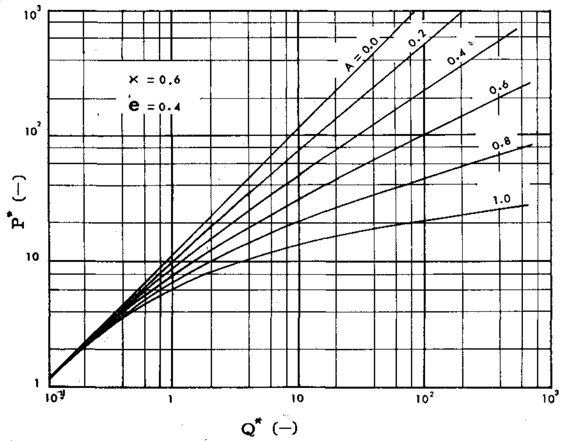

**Fig. 4 Iso-velocity lines, when $Re=0.0326$ ($\kappa=0.359$, $e=0.524$, $A=0.55$)**

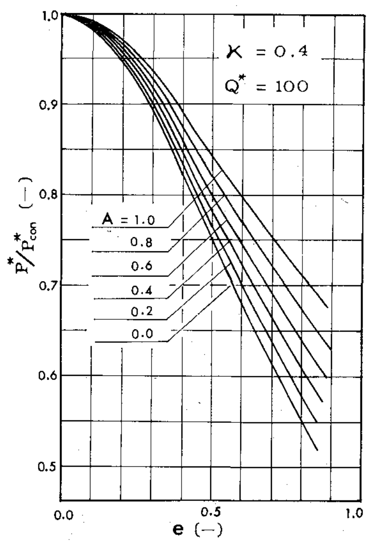

**Fig. 5 Variation of pressure drop with eccentricity ratio, when $\kappa=0.4$, $Q=100$**

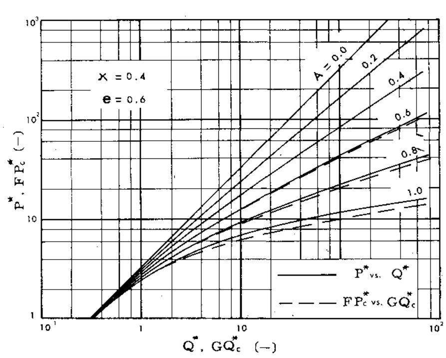

**Fig 6. Comparison of the flow curves obtained from Eqs.(47) and (50) with those due to variational calculation**

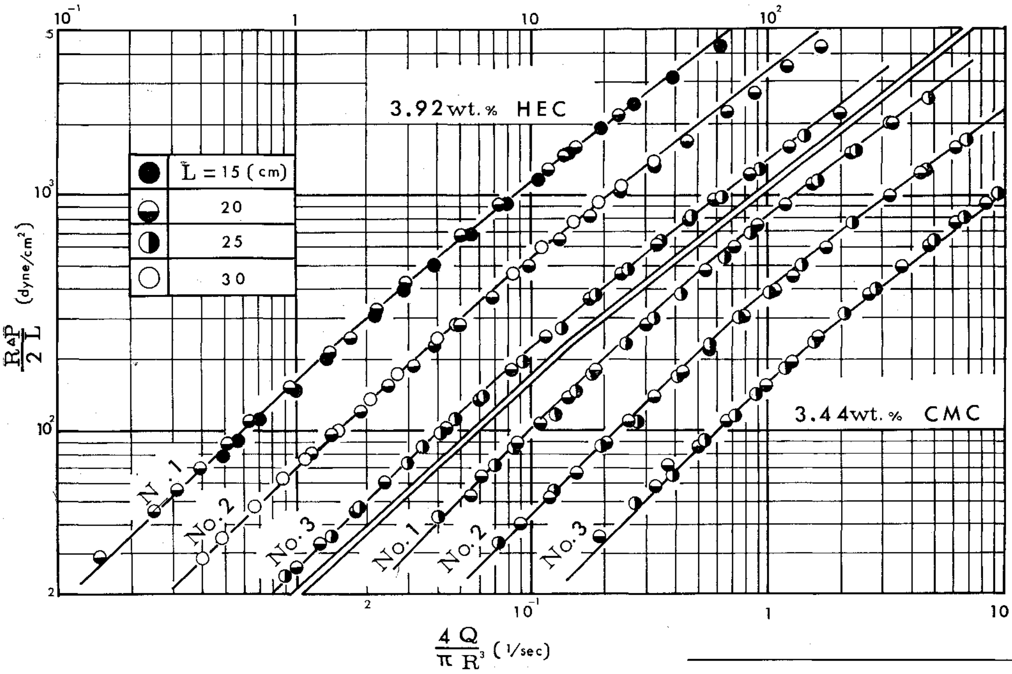


Solid lines are predictions by variational calculation.

**Fig. 7 Flow curves for 3.92 wt.% HEC and 3.44 wt.% CMC solutions flowing in eccentric annuli (No. 1, No. 3)**

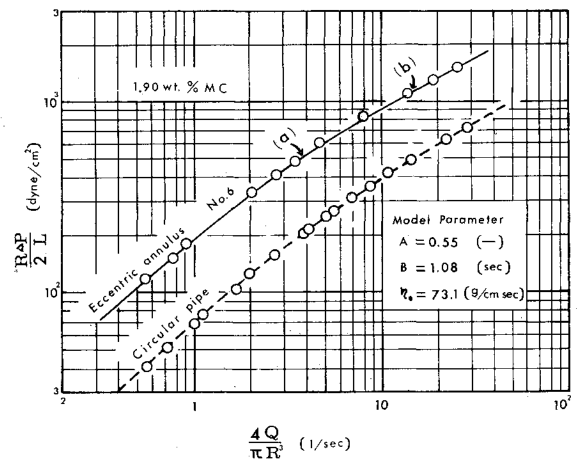


Solid line is prediction by variational calculation. Dashed line is flow curve of Sutterby model fluids ($A$=0.55, $B$=1.08, $\eta_0$=73.1) flowing in a circular pipe.

**Fig. 8 Flow curves for 1.90 wt.% MC solution flowing in an eccentric annulus (No. 6) and a circular pipe**

**Table 3** shows the Sutterby model parameters of the high-polymer aqueous solutions used in the experiment. These values were determined from the data for flow in a circular tube (Refer to the previous paper for details). **Figure 7** shows the experimental flow rate vs. pressure drop for 3.92 wt% HEC and 3.44 wt% CMC aqueous solutions in the eccentric annuli Nos. 1 through 3. The solid lines in the figure represent the results of applying the conventional variational method. They are in good agreement with the experimental data, even though they were estimated by a trial function which has one undetermined multiplier.

**Figure 8** shows the experimental data for 1.90 wt% MC aqueous solution in an eccentric annulus and in a circular tube. The constants in the Sutterby model were obtained by curves fitting the circular tube data. The solid lines in the figure represent the calculated values estimated by using these model parameters, and coincide with the experimental data.

**Table 3 Model parameters of fluid used in experiments**

| Fluid | $A$ [—] | $B$ [sec] | $\eta_0$ [g/cm·sec] |
|---|---|---|---|
| 2.50wt.% CMC | 0.60 | 0.121 | 9.52 |
| 3.44wt.% CMC | 0.45 | 0.715 | 71.5 |
| 3.92wt.% HEC | 0.30 | 0.368 | 12.1 |
| 4.50wt.% HEC | 0.30 | 0.299 | 13.1 |
| 1.90wt.% MC | 0.55 | 1.08 | 73.1 |

**Figures 9** and **10** show a comparison of the experimental velocity profiles with values calculated using the variational method for 1.90 wt% MC aqueous solution. Figure 9 shows the results for $Re$=0.0326 (point (a) in Fig. 8). The solid lines represent the calculated values. They agree well with the experimental data, as can be seen in these figures. On the other hand, for high Reynolds numbers, that is, highly non-Newtonian properties, even three undetermined multipliers in a trial function are not sufficient to estimate the velocity profiles. At the same time a relation between such macroscopic quantities as the flow rate and the pressure drop agree well with only one undetermined multiplier.

The predictions of Eqs.(47) through (50) were also compared with experimental results. If Eqs.(47) through (50) are approximately established, the experimental data ($R\Delta P/2L$) and ($4Q/\pi R^3$) for non-Newtonian flow through eccentric annuli having different ratios of inner and outer diameters and different eccentric ratios can be compared with those for non-Newtonian flow in a circular tube. **Figure 11** shows a plot of $(R\Delta P/2L)/F(\kappa, e)$ versus $(4Q/\pi R^3)/G(\kappa, e)$ in terms of experimental data in an eccentric annulus. It also shows a plot of ($R\Delta P/2L$) versus ($4Q/\pi R^3$) for flow in a circular tube. Each result for 2.50, 3.44 wt% CMC and 3.92, 4.50 wt% HEC aqueous solutions may be expressed by a single curve, and therefore Eqs.(47)

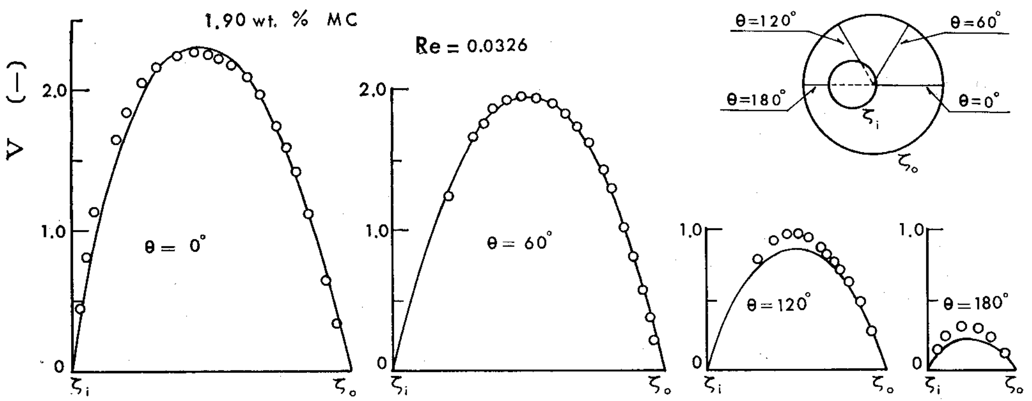


Solid lines are calculated velocity profiles. $Re$= 0.0326, which corresponds to point (a) on a flow curve in Fig. 8

**Fig. 9 Experimental data of velocity profiles for 1.90 wt.% MC solution flowing in an eccentric annulus (No. 6)**

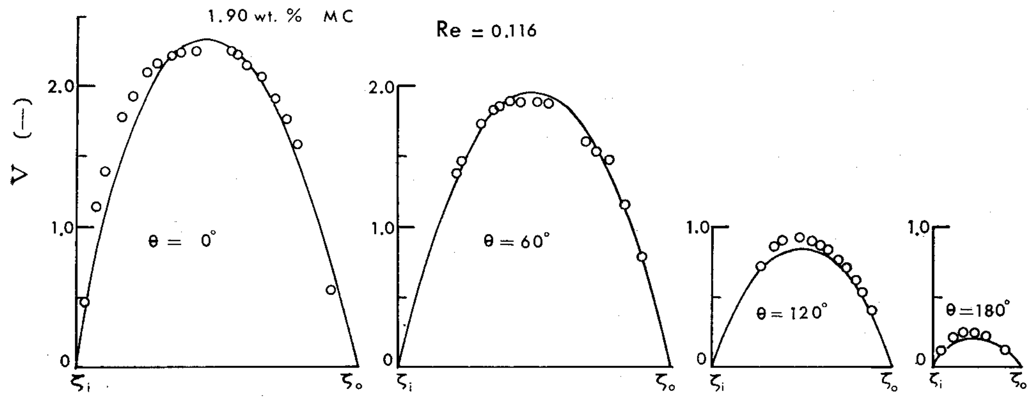


Solid lines are calculated velocity profiles. $Re$=0.116, which corresponds to point (b) on a flow curve in Fig. 8

**Fig. 10 Experimental data of velocity profiles for 1.90 wt.% MC solution flowing in an eccentric annulus (No. 6)**

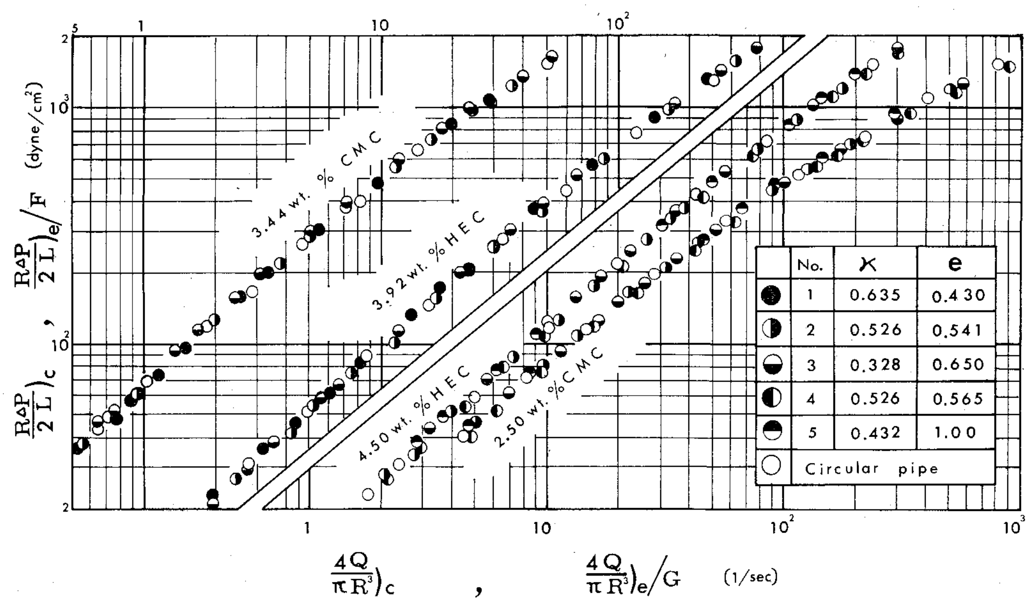


**Fig. 11 Comparison of Eqs.(47) and (50) with experimental data for the flows in annuli and circular pipes**

through (50) can be used for engineering calculations.

## 5. Secondary Flows in an Eccentric Annulus

Another important observation is the existence of secondary flows in an eccentric annulus. Since high-polymer aqueous solutions exhibit normal stress effects as well as non-Newtonian viscosity, variations in the $r$-component of velocity are possible. We have investigated the radial movement of hydrogen bubbles used as tracers. The flow patterns as shown in **Fig. 12** were observed for the case of Reynolds numbers larger than 0.01. We found that the radial velocity components of the secondary flows were always less than two percent of the average longitudinal velocity. We also found that no secondary flows could be observed for non-Newtonian flow in a concentric annulus or for Newtonian flow in an eccentric annulus. The secondary

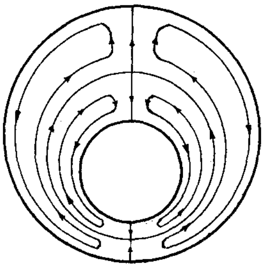

**Fig. 12 Secondary flow in an eccentric annulus**

flows observed are considered to be due to the normal stresses exhibited by viscoelastic fluid.

## 6. Summary

The relationship between flow rate and pressure drop, and velocity profiles is analyzed by the conventional variational method using the Sutterby non-Newtonian model for flow in an eccentric annulus.

The pressure drop for flow in an eccentric annulus decreases as the eccentricity increases at a fixed flow rate. Fluids with the stronger non-Newtonian property show a slower rate of decrease in pressure drop as eccentricity increases.

The calculated values for the dependence of flow rate on the pressure drop are in good agreement with our experimental data. The calculated values for the velocity profiles, on the other hand, show only fair agreement with the experimental data. However, good agreement is obtained for the not-so-strongly non-Newtonian fluids.

Eqs.(47) through (50) agree well with the experimental data. These equations may be useful for engineering calculations since the relation between flow rate and pressure drop in an eccentric annulus may be easily estimated in terms of experimental data for flow in a circular tube such as a capillary viscometer.

Secondary flows were observed, and are considered to be due to viscoelastic properties. But in the present work they are too small to contribute to the relation between flow rate and pressure drop.


### Acknowledgement

The authors are grateful to Professor R. B. Bird and his research group at the University of Wisconsin for their helpful advice.


## Nomenclature

| | | |
|---|---|---|
| $A$ | = constant in Sutterby model | [—] |
| $a_{i,1,2,3}$ | = unspecified parameter in trial function | [—] |
| $B$ | = constant in Sutterby model | [sec] |
| $b$ | = distance between centers of outer and inner tube | [cm] |
| $C$ | = constant defined by Eq.(1) | [cm] |
| $d_{ij}$ | = components of rate of deformation tensor | [1/sec] |
| $e$ | $= b/R(1-\kappa)$, eccentric ratio | [—] |
| $F$, $F(\kappa, e)$ | = shifter defined by Eq.(48) | [—] |
| $G$, $G(\kappa, e)$ | = shifter defined by Eq.(47) | [—] |
| $g_i$ | = components of gravitational force | [cm/sec$^2$] |
| $h$ | = metrical coefficients | [1/cm] |
| $h^*$ | $= Ch$ | [—] |
| $i$ | $= \sqrt{-1}$ | [—] |
| $J$ | = functional, Eq.(31) | [gcm/sec$^3$] |
| $L$ | = length of annular tube | [cm] |
| $P$ | = pressure drop | [dyne/cm$^2$] |
| $P^*$ | $= (B/\eta_0)(R\Delta P/2L)$, dimensionless pressure drop | [—] |
| $p$ | = pressure | [dyne/cm$^2$] |
| $Q$ | = volumetric flow rate | [cm$^3$/sec] |
| $Q^*$ | $= B(4Q/\pi R^3)$, dimensionless flow rate | [—] |
| $R$ | = radius of outer cylinder | [cm] |
| $Re$ | $= 2R(1-\kappa)\rho\langle v\rangle/\eta_0$, Reynolds number | [—] |
| $V$ | $= v/\langle v\rangle$, dimensionless velocity | [—] |
| $v_i$ | = components of velocity vector | [cm/sec] |
| $v$, $v_2$ | = velocity of $Z$ direction | [cm/sec] |
| $v_\xi$, $v_\zeta$ | = velocity of $\xi$, $\zeta$ direction | [cm/sec] |
| $\langle v\rangle$ | = mean velocity | [cm/sec] |
| $v^*$ | $= v/(C^2\Delta P/\eta_0 L)$, dimensionless velocity | [—] |
| $v_1^*$, $v_2^*$, $v_3^*$ | = 1st, 2nd, 3rd trial function of velocity | [—] |
| $x, y, z$ | = rectangular coordinates | [cm] |
| $\zeta$ | = bipolar cylindrical coordinate | [—] |
| $\eta$ | = non-Newtonian viscosity | [g/cm·sec] |
| $\eta_0$ | = zero-shear viscosity | [g/cm·sec] |
| $\eta^*$ | $= \eta/\eta_0$, dimensionless viscosity | [—] |
| $\kappa$ | = ratio of radius of inner cylinder to that of outer cylinder | [—] |
| $\nu$ | $= C/R$ | [—] |
| $\xi$ | = bipolar cylindrical coordinate | [—] |
| $\rho$ | = density | [g/cm$^3$] |
| $\tau_{\xi z}$, $\tau_{\zeta z}$ | = physical components of extra stress | [dyne/cm$^2$] |
| $\tau_{ij}$ | = components of extra stress tensor | [dyne/cm$^2$] |
| $\tau^*$ | $= (B/\eta_0)(C\Delta P/L)$ | [—] |

<Subscripts>

| | |
|---|---|
| $c$ | = circular pipe |
| $con$ | = concentric annulus |
| $e$ | = eccentric annulus |
| $i$ | = inner surface |
| $o$ | = outer surface |

<Special symbols>

| | | |
|---|---|---|
| II | = second invariant of $d_{ij}$, Eq.(17) | [1/sec$^2$] |
| II* | = dimensionless variable defined by Eq.(41) | [—] |

## Literature Cited


1) Asanuma, T.: *Journal of the J. S. M. E.*, **72**, 1370 (1969)
2) Happel, J. and H. Brenner: "Low Reynolds Number Hydrodynamics", p. 497, Prentice-Hall, Inc. (1965)
3) Miller, C.: *I. & E. C., Fundamentals*, **11**, 524 (1972)
4) Mitsuishi, N., Y. Kitayama and Y. Aoyagi: *Kagaku Kōgaku*, **31**, 570 (1967)
5) Mitsuishi, N. and Y. Aoyagi: Memoirs of the Faculty of Engineering, Kyushu University, **28**, 223 (1969)
6) Mitsuishi, N. and Y. Aoyagi: *Chem. Eng. Sci.*, **24**, 309 (1969)
7) Mitsuishi, N., Y. Aoyagi and H. Soeda: *Kagaku Kōgaku*, **36**, 182 (1972)
8) Mizushina, T., N. Mitsuishi and R. Nakamura: *Kagaku Kōgaku* (*Chem. Eng.*, Japan), **28**, 648 (1964)
9) Piercy, N. A. Y., M. S. Hooper and H. F. Winny; *Phil. Mag.* **15**, 647 (1933)
10) Redberger, P. J. and M. E. Charles: *Can. J. Chem. Eng.*, **40**, 148 (1962)
11) Schechter, R. S.: *AIChE J.*, **7**, 445 (1961)
12) Schechter, R. S.: "The Variational Method in Engineering", p, 80, McGraw Hill (1967)
13) Snyder, W. T. and G. A. Goldstein: *AIChE J.*, **11**, 462 (1965)
14) Sutterby, J. L.: *AIChE J.*, **12**, 63 (1966)
15) Wolffe, R. A. and C. W. Clump: *AIChE J.*, **9**, 424 (1963)